## Energy of a Prismatic Dislocation Loop in an Elastic Cylinder


Wei Cai and Christopher R. Weinberger



*Mathematics and Mechanics of Solids* 2009; 14; 192
DOI: 10.1177/1081286508092611

# Energy of a Prismatic Dislocation Loop in an Elastic Cylinder

WEI CAI
CHRISTOPHER R. WEINBERGER
*Department of Mechanical Engineering, Stanford University, CA 94305-4040, USA*

(Received 7 January 2008; accepted 10 January 2008)

*Abstract*: The energy of a prismatic dislocation loop in an isotropic elastic cylinder is derived, resulting in semi-analytic expressions. Analytic expressions are obtained in two limits: when the radius of the dislocation loop approaches the cylinder radius and when the radius of the dislocation loop is much smaller than the cylinder radius. These expressions can be used to predict the critical condition for misfit dislocation formation in semiconducting nanowires.

*Key Words*: Dislocation, Image stress, isotropic elasticity, Fourier transform

## 1. INTRODUCTION

Dislocations have been extensively studied because they are the fundamental carriers of plasticity in crystalline solids [1, 2]. Much of this progress has been made under the simplifying assumptions of linear elasticity, where the dislocation line is represented as a line singularity. This allows us to write the energy of a dislocation in an infinite medium as a line integral in terms of the infinite medium elastic Green function, which is available explicitly for isotropy.

Under the assumptions of isotropy, the stress field, energy and forces for special configurations can be derived. One such example is a circular prismatic loop, whose stress field and energy were derived by Kroupa [3]. Furthermore, some simple solutions are available for dislocations near free surfaces in both isotropic [4] and anisotropic [14] materials. Solutions for infinitely straight dislocations near flat free surfaces have obtained and used to predict the formation of misfit dislocations at the interface of hetero-epitaxial films [5, 6].

Much interest has been directed to the mechanical properties of cylindrical objects at the sub-micron scale, such as the single crystal metal pillars and nanowires [7, 8, 9]. In particular, Si and Ge nanowires with core-shell structures have recently been manufactured [10] and it is of interest to find out the critical condition for the generation of misfit dislocations at the cylindrical interface [11]. This analysis requires the energy of a prismatic dislocation loop inside an elastic cylinder, which does not exist to date.

In this paper, we derive a semi-analytic formula for the energy of a circular concentric prismatic dislocation loop in an elastically isotropic cylinder. The final expression involves one integral which can be computed very quickly by numerical quadrature. In addition, an-

*Mathematics and Mechanics of Solids* **14:** 192–206, 2009 DOI: 10.1177/1081286508092611

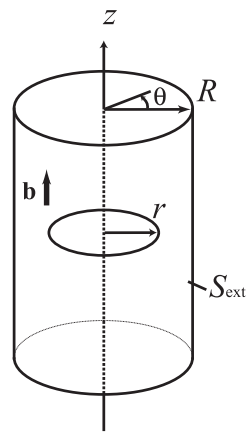


Figure 1. A circular prismatic dislocation loop inside an elastic cylinder.

alytic expressions are obtained in two limits: when the radius of the dislocation loop approaches the cylinder radius and when the radius of the dislocation loop is much smaller than the cylinder radius.

Because the energy of a prismatic dislocation loop is available analytically, Section 1 derives the energy change of the dislocation loop due to the presence of a cylindrical free surface, which we will call the image energy, using the Fourier transform method. The image energy gives rise to an image force, which is equivalent to the Peach Koehler force from the image stress [15]. Section 2 gives the analytic expressions of the elastic energy in the two asymptotic limits. Section 3 gives a brief summary and outlook of future research along this line. For readability, most of the detailed derivations are given in the appendices.

## 2. IMAGE ENERGY OF A DISLOCATION LOOP

### *2.1. Geometry and Scaling Relations*

The self energy of a circular edge dislocation loop of radius $r$ in an infinite isotropic elastic medium with shear modulus $\mu$ and Poisson's ratio $\nu$ has been obtained by Kroupa [3]:

$$E^{\infty} = 2\,\pi\, r\, \frac{\mu\, b^2}{4\pi\,(1-\nu)} \left( \ln \frac{8r}{r_c} - 1 \right) \tag{1}$$

where $b$ is the magnitude of the Burgers vector whose orientation is orthogonal to the dislocation loop and $r_c$ is a short-range cut-off parameter (dislocation core radius) introduced to avoid the singularity in continuum elasticity theory. Because the dislocation line length is $2\pi r$, the terms behind $2\pi r$ can be considered as the energy per unit length.

We now consider the same dislocation loop inside an infinitely long elastic cylinder of radius $R$ where both the cylinder axis and the dislocation Burgers vector coincide with the $z$-axis, as shown in Figure 1. Let $E^{\text{tot}}$ be the elastic energy of this dislocation loop, and define $E^{\text{img}}$ as the difference between $E^{\text{tot}}$ and $E^{\infty}$, i.e.

$$E^{\text{tot}} = E^{\infty} + E^{\text{img}} \tag{2}$$

In other words, $E^{\text{img}}$ describes the energy change of the dislocation loop due to the introduction of the free surface of the cylinder. We call $E^{\text{img}}$ the *image energy*, and it can be shown that $E^{\text{img}} < 0$.

When the elastic constants $\mu$, $\nu$ and Burgers vector $b$ are given, $E^{\infty}$ is only a function of $r$ and $r_c$, i.e. $E^{\infty}(r, r_c)$. We will see shortly that $E^{\text{img}}$ is only a function of $r$ and $R$, i.e.

$$E^{\text{tot}}(r, R, r_c) = E^{\infty}(r, r_c) + E^{\text{img}}(r, R). \tag{3}$$

Since continuum elasticity theory does not have an intrinsic length scale, $E^{\text{tot}}(r, R, r_c)$ must satisfy certain scaling relationships. Specifically, it can be shown that

$$E^{\text{tot}}(\lambda r, \lambda R, \lambda r_c) = \lambda E^{\text{tot}}(r, R, r_c) \tag{4}$$

$$E^{\infty}(\lambda r, \lambda r_c) = \lambda E^{\infty}(r, r_c) \tag{5}$$

$$E^{\text{img}}(\lambda r, \lambda R) = \lambda E^{\text{img}}(r, R). \tag{6}$$

In other words, $E^{\text{tot}}(r, R, r_c)$, $E^{\infty}(r, r_c)$ and $E^{\text{img}}(r, R)$ are homogeneous functions of order 1.

Because an analytic expression is available for $E^{\infty}$, our task amounts to the determination of the image energy $E^{\text{img}}$. Due to the scaling relation given by Equation (6), the image energy can be reduced to a one-dimensional function,

$$E^{\text{img}}(r, R) = E^{\text{img}}\left(\frac{R}{r}\right) \cdot r. \tag{7}$$

This means that we can fix the dislocation loop radius at $r = 1$ without loss of generality, and derive the expression of $E^{\text{img}}$ as a function of $R$ for $1 < R < \infty$. This result can then be used to construct $E^{\text{img}}(r, R)$ for arbitrary $r$ and $R$.

### *2.2. Image Energy as a Surface Integral*

We now fix $r = 1$ and examine $E^{\text{img}}$ as a function of $R$ for $1 < R < \infty$. In [12], we have derived an expression for the image energy in terms of an integral over the cylindrical surface,

$$E^{\text{img}}(R) = -\frac{1}{2} \iint_{S_{\text{ext}}} \mathbf{T}^R(z, \theta) \cdot \left[\left|\mathbf{u}^R\right|\right](z, \theta)\, \mathrm{d}S. \tag{8}$$

This is the starting point of our derivation here. In the following, we briefly explain the various terms and the physical meaning of this equation.

Consider the following steps to construct the stress field of a circular prismatic dislocation loop inside an elastic cylinder. *In the first step*, we consider the stress field of the dislocation loop inside an infinite medium, $\sigma_{ij}^{\infty}$. To satisfy equilibrium, traction forces

$F_j = \sigma^{\infty}_{ij} n_i$ need to be applied to the cylinder surface, where $n_i$ is the local (outward) normal vector of the surface. *In the second step*, the surface tractions are removed so that the cylinder satisfies the zero-traction boundary condition. This can be done by superimposing another solution, which corresponds to a dislocation-free cylinder subjected to surface traction $T_j = -F_j = -\sigma^{\infty}_{ij} n_i$. The stress field produced by $T_j$ is called the image stress $\sigma^{\text{img}}_{ij}$. The total stress field of interest is then

$$\sigma^{\text{tot}}_{ij} = \sigma^{\infty}_{ij} + \sigma^{\text{img}}_{ij}. \tag{9}$$

$T_j$ (index form) is the same as $\mathbf{T}^R$ (vector form) in Equation (8). The superscript $^R$ is added to signify that the quantity is defined at the cylinder surface of radius $R$.

In order to construct the image energy, we consider both an infinite cylinder and a body with an infinite cylindrical hole. The union of these two domains creates an infinite body. When a dislocation-free cylinder is subjected to the surface tractions $\mathbf{T}^R$, the corresponding displacements on the surface are $\overline{\mathbf{u}}_c$. Also, when the inner surface of the hole is subjected to the surface tractions $-\mathbf{T}^R$, the corresponding displacements on the surface are $\overline{\mathbf{u}}_h$. $\left[\left|\mathbf{u}^R\right|\right]$ in Equation (8) is simply the difference between $\overline{\mathbf{u}}_c$ and $\overline{\mathbf{u}}_h$:

$$\left[\left|\mathbf{u}^R\right|\right] \equiv \overline{\mathbf{u}}_c - \overline{\mathbf{u}}_h \tag{10}$$

in cylindrical coordinates.

The physical meaning of Equation (8) can be interpreted by the following thought experiment in which an infinite medium containing a dislocation loop is transformed into a cylinder containing the same dislocation loop. *In the first step*, a cylinder (containing the dislocation loop) is cut out from the infinite medium. External traction forces are applied to the outer surface of the cylinder and the inner surface of the cylindrical hole. *In the second step*, these forces are slowly reduced to zero. The right-hand side of Equation (8) is precisely the work done by the (external) surface traction forces in the second step.

Given the symmetry of our problem, both $\mathbf{T}^R$ and $\left[\left|\mathbf{u}^R\right|\right]$ are independent of $\theta$ when they are expressed in cylindrical coordinates. (Their $\theta$ components are also zero.) Therefore, $E^{\text{img}}$ is reduced to a one-dimensional integral along $z$,

$$E^{\text{img}}(R) = -\pi\, R \int_{-\infty}^{\infty} \mathbf{T}^R(z) \cdot \left[\left|\mathbf{u}^R\right|\right](z)\, \mathrm{d}z. \tag{11}$$

Defining the Fourier transform of $\mathbf{T}^R(z)$ and $\left[\left|\mathbf{u}^R\right|\right](z)$ as,

$$\hat{\mathbf{T}}^R(k_z) \equiv \int_{-\infty}^{\infty} \mathbf{T}^R(z)\, \mathrm{e}^{-\mathrm{i}k_z z}\, \mathrm{d}z \quad \mathbf{T}^R(z) = \frac{1}{2\pi} \int_{-\infty}^{\infty} \hat{\mathbf{T}}^R(k_z)\, \mathrm{e}^{\mathrm{i}k_z z}\, \mathrm{d}z \tag{12}$$

$$\left[\left|\hat{\mathbf{u}}^R\right|\right](k_z) \equiv \int_{-\infty}^{\infty} \left[\left|\mathbf{u}^R\right|\right](z)\, \mathrm{e}^{-\mathrm{i}k_z z}\, \mathrm{d}z$$

$$\left[\left|\mathbf{u}^R\right|\right](z) = \frac{1}{2\pi} \int_{-\infty}^{\infty} \left[\left|\hat{\mathbf{u}}^R\right|\right](k_z)\, \mathrm{e}^{\mathrm{i}k_z z}\, \mathrm{d}z \tag{13}$$

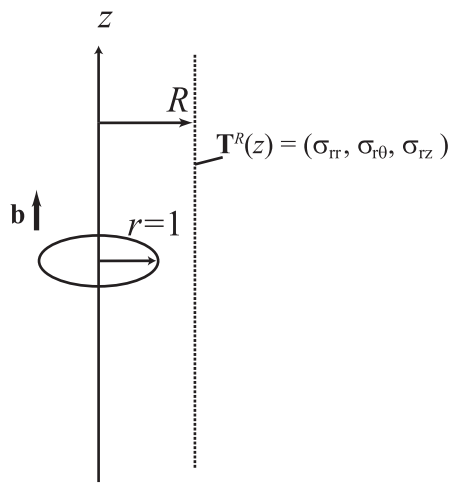


Figure 2. $\mathbf{T}^R(z)$ corresponds to three stress components of a circular prismatic dislocation loop in an infinite medium on a cylindrical surface with radius $R$.

then by Parseval's Theorem, the image energy can be also be written as

$$E^{\text{img}}(R) = -\frac{R}{2}\int_{-\infty}^{\infty} (\hat{\mathbf{T}}^R(k_z))^* \cdot \left[\left|\hat{\mathbf{u}}^R\right|\right](k_z)\, \mathrm{d}k_z \tag{14}$$

where $^*$ represents the complex conjugate.

### *2.3. Stress Field of a Circular Prismatic Dislocation Loop*

In order to obtain the image energy, we now need $\hat{\mathbf{T}}^R(k_z)$ and $\left[\left|\hat{\mathbf{u}}^R\right|\right](k_z)$. $\hat{\mathbf{T}}^R(k_z)$ is simply the Fourier transform of the stress field of a prismatic dislocation loop along the $z$ direction evaluated at $R$. $\left[\left|\hat{\mathbf{u}}^R\right|\right](k_z)$ can be then obtained from $\hat{\mathbf{T}}^R(k_z)$ using the transformations derived in [12].

The stress field of a prismatic dislocation loop has been obtained by Kroupa [3], but the result is written in the form of a Laplace transform. Instead of converting Kroupa's solution to the Fourier space, for this application it is easier to solve this problem again using the Fourier method. The relevant traction components on the cylinder surface are (for $k_z > 0$)

$$\begin{aligned}
\hat{T}_r^R(k_z) &= -\frac{\mathrm{i}\pi\mu b}{2(1-\nu)R}\left[2(1-\nu)H_1^R J_1 - \mathrm{i}k_z(RH_0^R J_1 + H_1^R J_0)\right. \\
&+ \left. k_z^2 R(RH_1^R J_1 - H_0^R J_0)\right] \\
\hat{T}_\theta^R(k_z) &= 0 \\
\hat{T}_z^R(k_z) &= \frac{\mathrm{i}\pi\mu b k_z^2}{2(1-\nu)}\left[RH_0^R J_1 + H_1^R J_0\right]
\end{aligned} \tag{15}$$

where

$$\begin{aligned} &J_0 \equiv J_0(\mathrm{i}k_z) \quad J_1 \equiv J_1(\mathrm{i}k_z) \quad H_0 \equiv H_0^{(1)}(\mathrm{i}k_z) \quad H_1 \equiv H_1^{(1)}(\mathrm{i}k_z) \\ &J_0^R \equiv J_0(\mathrm{i}k_z R) \quad J_1^R \equiv J_1(\mathrm{i}k_z R) \quad H_0^R \equiv H_0^{(1)}(\mathrm{i}k_z R) \quad H_1^R \equiv H_1^{(1)}(\mathrm{i}k_z R) \end{aligned} \tag{16}$$

$J_{0,1}(\cdot)$ are Bessel functions and $H_{0,1}^{(1)}(\cdot)$ are Hankel functions of the first kind. The derivation details are given in Appendix A. For $k_z > 0$, $J_0$, $J_0^R$, $H_1$, $H_1^R$ are real numbers, and $J_1$, $J_1^R$, $H_0$, $H_0^R$ are imaginary numbers. If we change $k_z$ to $-k_z$, the values of $J_0$, $J_0^R$, $H_1$, $H_1^R$, $J_1$, $J_1^R$, $H_0$, $H_0^R$ change to their complex conjugate values. From $\hat{\mathbf{T}}^R(k_z)$ we obtain $\left[\left|\hat{\mathbf{u}}\right|\right](k_z)$ using the results in [12].

$$\begin{aligned} \left[\left|\hat{u}_r^R\right|\right](k_z) &= \mathrm{i}k_z\, b \cdot \frac{R J_0^R J_1 - J_1^R J_0}{2(1-\nu) J_1^{R2} + (J_0^{R2} + J_1^{R2}) k_z^2 R^2} \\ \left[\left|\hat{u}_\theta^R\right|\right](k_z) &= 0 \\ \left[\left|\hat{u}_z^R(k_z)\right|\right] &= -\frac{\mathrm{i}\, b}{k_z R} \cdot \frac{2(1-\nu) J_1^R J_1 - \mathrm{i}k_z (R J_0^R J_1 - J_1^R J_0) + k_z^2 R (R J_1^R J_1 + J_0^R J_0)}{2(1-\nu) J_1^{R2} + (J_0^{R2} + J_1^{R2}) k_z^2 R^2}. \end{aligned} \tag{17}$$

$\hat{T}_r^R(k_z)$ and $\left[\left|\hat{u}_r^R\right|\right](k_z)$ are real numbers, while $\hat{T}_z^R(k_z)$ and $\left[\left|\hat{u}_z^R\right|\right](k_z)$ are imaginary numbers, thus ensuring $E^{\mathrm{img}}$ is real. The final expression for $E^{\mathrm{img}}$ is

$$\begin{aligned} E^{\mathrm{img}} &= R \int_0^\infty \left\{ -\left[\left|\hat{u}_r^R\right|\right](k_z) \hat{T}_r^R(k_z) + \left[\left|\hat{u}_z^R\right|\right](k_z) \hat{T}_z^R(k_z) \right\} \mathrm{d}k_z \\ &= \frac{\mu\, b^2}{2(1-\nu)} \int_0^\infty \frac{P(R, k_z)}{Q(R, k_z)} \mathrm{d}k_z \end{aligned} \tag{18}$$

$$\begin{aligned} P(R, k_z) &= 2\pi R^2 k_z^3 (H_0^R J_0^R + H_1^R J_1^R) J_0 J_1 + 2R^2 k_z^2 J_1^2 - 2k_z^2 J_0^2 \\ &+ 4(1-\nu) J_1^2 + 4\pi (1-\nu)\, k_z\, H_1^R J_1^R J_0 J_1 \\ Q(R, k_z) &= 2(1-\nu) J_1^{R2} + (J_0^{R2} + J_1^{R2}) k_z^2 R^2. \end{aligned} \tag{19}$$

Here we have used the fact that the integrand is an even function of $k_z$. The derivation details are given in Appendix B.

## 3. THE FUNCTIONAL BEHAVIOR OF $E^{\mathrm{img}}(r, R)$

### 3.1. $E^{\mathrm{img}}(r = 1, R)$ *for* $1 < R < \infty$

By definition, $E^{\mathrm{img}}$ should go to zero when $R/r \to \infty$. By taking the limit as $R \to \infty$ in Equation (18), we find that

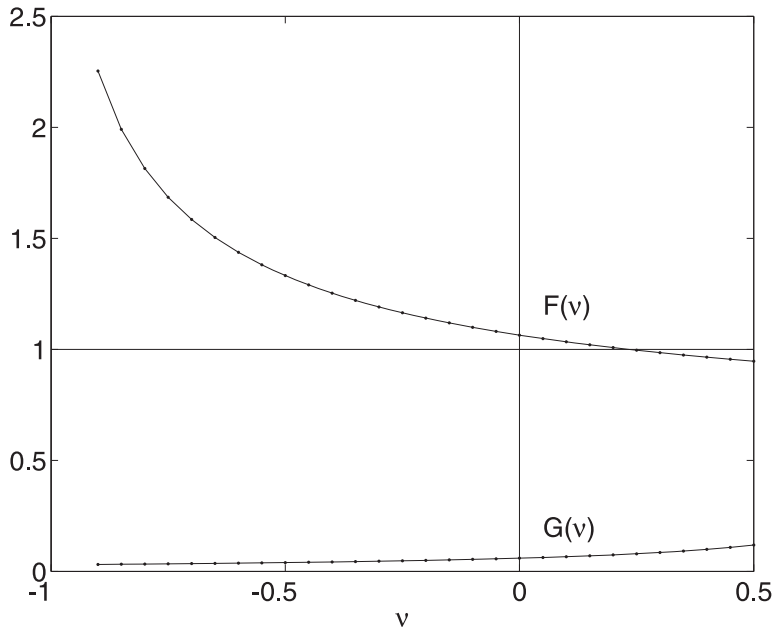


Figure 3. Functions $F(\nu)$ and $G(\nu)$ for $-1 < \nu < 0.5$, which appear in the expression of image energy in the asymptotic limits of $R \to \infty$ and $R \to 1$, Equations (20) and (21).

$$\frac{E^{\text{img}}(r = 1, R)}{\mu\, b^2} \to -\frac{F(\nu)}{1-\nu} \cdot \frac{1}{R^3} \quad R \to \infty \tag{20}$$

where the analytic expression for $F(\nu)$ and the associated details are given in Appendix C. The numerical values of $F(\nu)$ are plotted in Figure 3. We observe that $F(\nu) \approx 1$ for $0.2 \leq \nu \leq 0.3$.

We also expect $E^{\text{img}} \to -\infty$ in the limit of $R \to r$. Taking the limit as $R \to 1$ in Equation (18), we find that

$$\frac{E^{\text{img}}(r = 1, R)}{\mu\, b^2} \to \frac{1}{2(1-\nu)} \ln(R-1) + G(\nu) \quad R \to 1 \tag{21}$$

where the analytic expression for $G(\nu)$ and the associated details are given in Appendix D. The numerical values of $G(\nu)$ are plotted in Figure 3. We observe that $G(\nu) \approx 0$ for $0.2 \leq \nu \leq 0.3$.

From Equation (18), we can see that $E^{\text{img}}$ depends linearly on $\mu$ and $b^2$. However, the dependence of the image energy on $R/r$ and $\nu$ is non-trivial. For a given Poisson's ratio $\nu$, $E^{\text{img}}(r = 1, R)$ can be easily computed as a function of $R$ by numerical integration of Equation (18). Figure 4 plots this function for the case of $\nu = 0.2$, along with the asymptotic limits at $R \to \infty$ and $R \to 1$. (The Poisson's ratio is 0.200 for Ge and 0.218 for Si.) The numerical results confirm the asymptotic formulae of Equations (20)–(21).

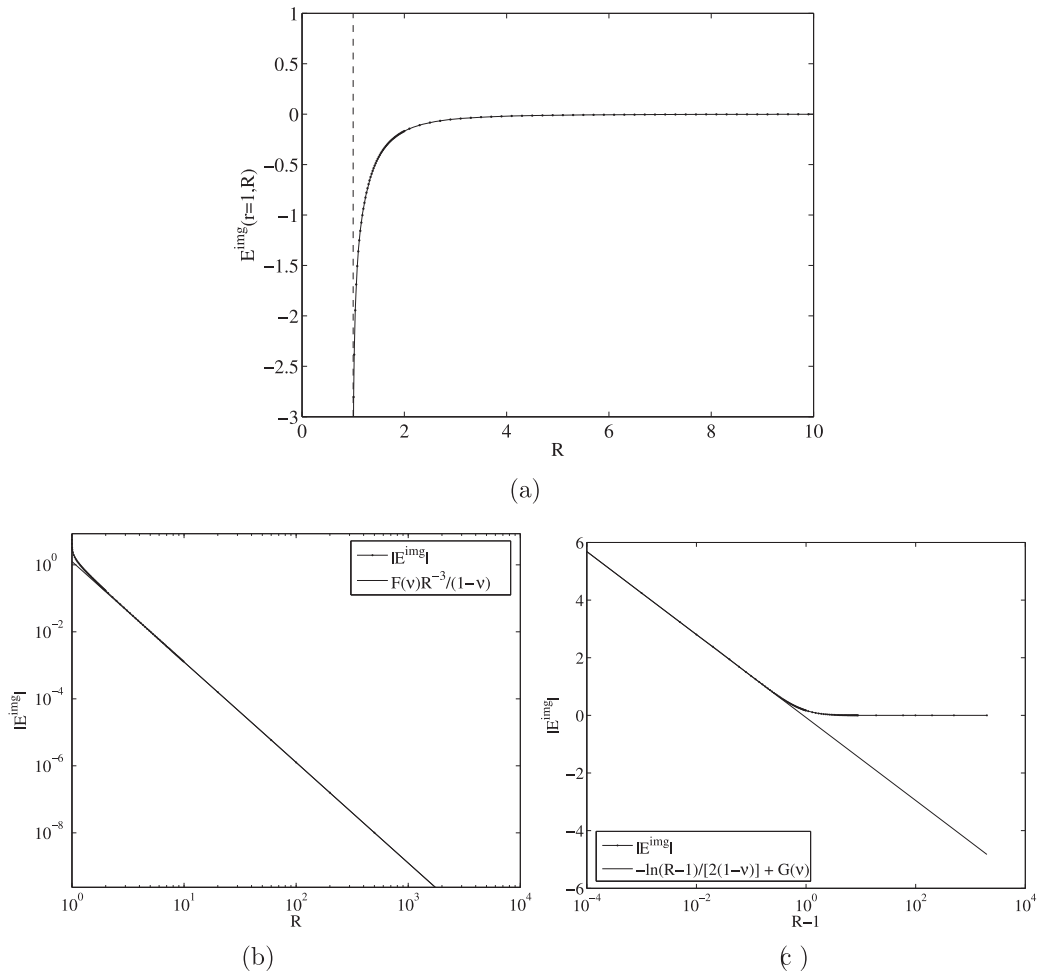


Figure 4. (a) The image energy $E^{\text{img}}(r, R)$ as a function of the cylinder radius $R$ at a dislocation loop radius of $r = 1$ and a Possion's ratio of $\nu = 0.2$. (b) Comparison between $E^{\text{img}}(r, R)$ and Equation (20) in the limit of $R \to \infty$. (c) Comparison between $E_{\text{img}}(r, R)$ and Equation (21) in the limit of $R \to 1$.

### 3.2. $E^{\text{img}}(r, R = 1)$ *for* $0 < r < 1$

Given the scaling relation, Equation (6), we can easily obtain the dependence of $E^{\text{img}}$ on $r$ at $R = 1$, given $E^{\text{img}}(r = 1, R)$, i.e.

$$E^{\text{img}}(r, R = 1) = E^{\text{img}}(1, R = 1/r) \cdot r. \tag{22}$$

This means that in the limit of $r \to 0$,

$$\frac{E^{\text{img}}(r, R = 1)}{\mu\, b^2} \to -\frac{F(\nu)}{1 - \nu} \cdot r^4 \quad r \to 0. \tag{23}$$

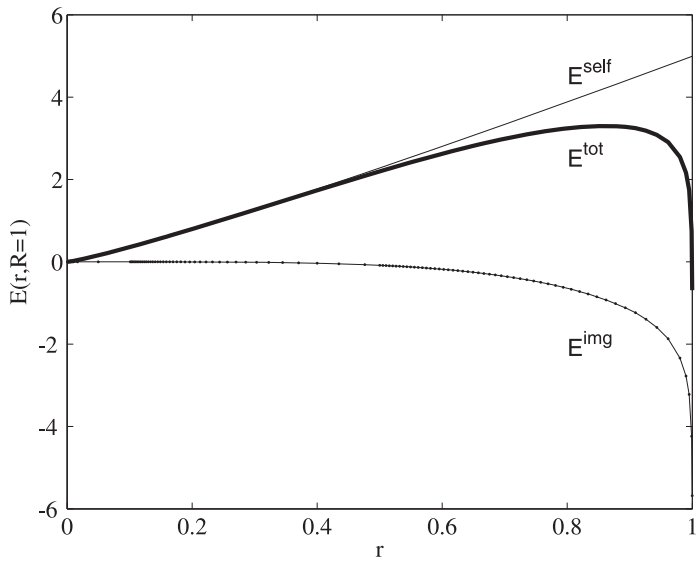


Figure 5. The image energy $E^{\text{img}}$, self-energy $E^{\text{self}}$ and total energy $E^{\text{tot}}$ of the dislocation loop as a function of loop radius $r$ in a cylinder with radius $R = 1$.

In the limit of $r \to 1$,

$$\frac{E^{\text{img}}(r, R = 1)}{\mu\, b^2} \to \frac{1}{2(1-\nu)} \ln(1-r) + G(\nu) \quad r \to 1. \tag{24}$$

Consequently, as $r \to 1$, the image force (per unit length) on the dislocation loop becomes

$$f^{\text{img}} \to \frac{\mu\, b^2}{4\pi\,(1-\nu)} \cdot \frac{1}{1-r} \tag{25}$$

which is the same as the Peach–Koehler force exerted between two straight dislocations with opposite Burgers vectors that are separated by $2(1-r)$. This distance is precisely twice the distance between the dislocation loop (radius $r$) and the cylindrical surface (radius $R = 1$). This form of image force was correctly proposed by [11], for which our derivation can be regarded as a formal proof.

The image energy as a function of $r$ is plotted in Figure 5 for the case of $\nu = 0.2$. The self-energy and the total energy of the dislocation loop are also plotted in the same figure. While $E^{\text{self}}$ monotonically increases with $r$ and $E^{\text{img}}$ monotonically decreases with $r$, the total energy $E^{\text{tot}}$ exhibits a maximum at $r \approx 0.8$. The location of the maximum depends on the values of core radius $r_c$ and Poisson's ratio $\nu$.

## 4. SUMMARY AND OUTLOOK

Here we have derived a semi-analytical formula for the energy of a prismatic dislocation loop inside an elastically isotropic cylinder. The result is expressed in terms of a one-dimensional integral that can be easily evaluated by numerical quadrature. We have also found simple analytic expressions for the two important limits: when the dislocation loop radius approaches the cylinder radius and when loop radius is much smaller than the cylinder radius. These results can be used to predict the critical condition for the nucleation of misfit dislocations in cylindrical core-shell hetero-epitaxial structures. The derivation here can be slightly modified to give the energy of a periodic array of dislocation loops in which the integral would be replaced by a series. This procedure can also be generalized to derive the energy of glide dislocation loops whose glide plane normal tilts away from the cylinder axis.

*Acknowledgments. The authors wish to thank Professor D. M. Barnett and Professor W. D. Nix for useful discussions. The work is supported by a NSF Career grant CMS-0547681, a AFOSR/YIP grant and by the Army High Performance Computing Research Center at Stanford. C. R. Weinberger is supported by a Benchmark Stanford Graduate Fellowship.*

## APPENDIX A. STRESS FIELD OF PRISMATIC DISLOCATION LOOP IN FOURIER SPACE

Here we drive the stress field of a prismatic dislocation loop in an infinite medium using the Fourier method. To do this, we first consider a dislocation loop with a radius $r = 1$ shown in Figure 2. This dislocation loop is equivalent to a displacement jump across the cylindrical surface $r = 1$ that is a step function in $z$,

$$\left[\left|u_z\right|\right](z) \equiv u_z(r = 1^-, z) - u_z(r = 1^+, z) = b\, h(z) \tag{A.1}$$

where $h(z)$ is the Heaviside function, i.e. $h(z) = 0$ for $z < 0$ and $h(z) = 1$ for $z > 0$. Here the superscript $^R$ is omitted on $\left[\left|u_z\right|\right]$ because the displacement jump is evaluated at radius $r = 1$, instead of at radius $R$. The Fourier transform of $\left[\left|u_z\right|\right](z)$ is

$$\left[\left|\hat{u}_z\right|\right](k_z) \equiv \int_{-\infty}^{\infty} \left[\left|u_z\right|\right](z)\, \mathrm{e}^{-\mathrm{i}k_z z}\, \mathrm{d}z = -\frac{\mathrm{i}\, b}{k_z} + \pi\, \delta(k_z). \tag{A.2}$$

The $\pi\, \delta(k_z)$ can be ignored because it corresponds to a uniform sliding between the inside and the outside of the cylindrical surface and does not generate any stress field. According to [12], the traction force across the cylindrical interface at $r = 1$ can be easily obtained in Fourier space:

$$\begin{aligned}
\hat{T}_r(k_z) &= -\frac{\mathrm{i}\pi\, \mu\, b}{2(1-\nu)} \left[2(1-\nu) H_1 J_1 - \mathrm{i}k_z (H_0 J_1 + H_1 J_0) + k_z^2 (H_1 J_1 - H_0 J_0)\right] \\
\hat{T}_\theta(k_z) &= 0 \qquad\qquad (A.3) \\
\hat{T}_z(k_z) &= \frac{\mathrm{i}\pi\, \mu\, b\, k_z^2}{2(1-\nu)} \left[H_0 J_1 + H_1 J_0\right].
\end{aligned}$$

If we take the inverse Fourier transform of the above three functions, we will obtain three stress components, $\sigma_{rr}$, $\sigma_{r\theta}$ and $\sigma_{rz}$ on the cylinder $r = 1$, as functions of $z$.

Our next step is to obtain the same three stress components at a larger cylindrical surface at radius $R$. To do so, we need to know how the stress field decays outside the cylinder of $r = 1$. According to [12], a general (Fourier mode) solution for the displacement field in an infinite medium is

$$\mathbf{u} = \nabla\phi + \nabla \times \boldsymbol{\psi} \tag{A.4}$$

where $\phi$ and $\boldsymbol{\psi}$ are scalar and vector potentials [13] that can be expressed as

$$\phi = \frac{1-2\nu}{2(1-\nu)}\left[A\, r \frac{\mathrm{d}}{\mathrm{d}r} H_n^{(\alpha)}(\mathrm{i}k_z r)\right] \mathrm{e}^{\mathrm{i}n\theta + \mathrm{i}k_z z} \tag{A.5}$$

$$\psi_r = \left[\mathrm{i}\, B\, H_{n+1}^{(\alpha)}(\mathrm{i}k_z r) - \mathrm{i}A\, r \frac{\mathrm{d}}{\mathrm{d}r} H_{n+1}^{(\alpha)}(\mathrm{i}k_z r)\right] \mathrm{e}^{\mathrm{i}n\theta + \mathrm{i}k_z z} \tag{A.6}$$

$$\psi_\theta = \left[B\, H_{n+1}^{(\alpha)}(\mathrm{i}k_z r) - A\, r \frac{\mathrm{d}}{\mathrm{d}r} H_{n+1}^{(\alpha)}(\mathrm{i}k_z r)\right] \mathrm{e}^{\mathrm{i}n\theta + \mathrm{i}k_z z} \tag{A.7}$$

$$\psi_z = \left[\mathrm{i}\, C\, H_n^{(\alpha)}(\mathrm{i}k_z r) + \mathrm{i}A\, r \frac{\mathrm{d}}{\mathrm{d}r} H_n^{(\alpha)}(\mathrm{i}k_z r)\right] \mathrm{e}^{\mathrm{i}n\theta + \mathrm{i}k_z z}. \tag{A.8}$$

$A$, $B$, $C$ are three coefficients for this Fourier mode that can be used to satisfy three boundary conditions. $H_n^{(\alpha)}(\cdot)$, $\alpha = 1, 2$ are Hankel functions of the first and second kind with $\alpha = 1$ for $k_z > 0$ and $\alpha = 2$ for $k_z < 0$. Since this solution decays to zero as $r \to \infty$, it is suitable to describe the displacement field outside a cylindrical region of an infinite medium. Due to the axial symmetry of our problem, we are only interested in the case of $n = 0$.

Given the above expressions for the displacement field, we can obtain the relationship between three stress components (or traction forces) at cylinder surface $r = 1$ and the coefficients $A$, $B$, $C$. This relationship can be summarized by a matrix $\mathbf{M}'$:

$$\begin{pmatrix} \hat{T}_r \\ \hat{T}_\theta \\ \hat{T}_z \end{pmatrix} = \mathbf{M}' \cdot \begin{pmatrix} A \\ B \\ C \end{pmatrix}. \tag{A.9}$$

Similarly, we can obtain the relationship between the same stress components at the cylindrical surface with radius $R$ and the coefficients $A$, $B$, $C$:

$$\begin{pmatrix} \hat{T}_r^R \\ \hat{T}_\theta^R \\ \hat{T}_z^R \end{pmatrix} = \mathbf{M}'^R \cdot \begin{pmatrix} A \\ B \\ C \end{pmatrix}. \tag{A.10}$$

Therefore, the traction forces at the radius $R$ can be written in terms of those at the radius $r = 1$ as

$$\begin{pmatrix} \hat{T}_r^R \\ \hat{T}_\theta^R \\ \hat{T}_z^R \end{pmatrix} = \mathbf{M}'^R \cdot \left(\mathbf{M}'\right)^{-1} \cdot \begin{pmatrix} \hat{T}_r \\ \hat{T}_\theta \\ \hat{T}_z \end{pmatrix}. \tag{A.11}$$

The analytic expression for matrix $\mathbf{M}'$ is given in [12]. The expression for the matrix $\mathbf{M}'^R$ can be obtained from that of the matrix $\mathbf{M}'$ by substituting $k_z \to k_z R$, and multiplying by $1/R^2$ whose result is Equation (15). It can be easily verified that in the limit of $R \to 1$, Equation (15) reduces to Equation (A.3).

## APPENDIX B. THE DETAILS OF THE IMAGE ENERGY DERIVATION

In [12], it was shown that, for every Fourier mode, the relationship between the displacement jump and the traction force across the cylindrical surface ($r = 1$) can be written in the matrix form

$$\left[\left|\hat{\mathbf{u}}\right|\right] = \left(\mathbf{N}\,\mathbf{M}^{-1} - \mathbf{N}'\,\mathbf{M}'^{-1}\right)\hat{\mathbf{T}}. \tag{B.1}$$

The analytic expressions for matrices $\mathbf{M}$, $\mathbf{N}$, $\mathbf{M}'$, $\mathbf{N}'$ are given in [12]. A similar relationship exists at a different cylindrical surface with radius $R$:

$$\left[\left|\hat{\mathbf{u}}^R\right|\right] = \left(\mathbf{N}^R\,(\mathbf{M}^R)^{-1} - \mathbf{N}'^R\,(\mathbf{M}'^R)^{-1}\right)\hat{\mathbf{T}}^R. \tag{B.2}$$

The expression for matrix $\mathbf{M}'^R$ and $\mathbf{N}'^R$ can be obtained from that of matrix $\mathbf{M}'$ and $\mathbf{N}'$, respectively, by substituting $k_z \to k_z R$ and multiplying the result by $1/R^2$.

Given the expression for $\hat{\mathbf{T}}^R$, shown in Equation (15), we can obtain the expression for $\left[\left|\hat{\mathbf{u}}^R\right|\right]$ through Equation (B.2). The result is given in Equation (17).

The image energy is given by Equation (14) as

$$E^{\text{img}}(R) = -\frac{R}{2}\int_{-\infty}^{\infty} (\hat{\mathbf{T}}^R(k_z))^* \cdot \left[\left|\hat{\mathbf{u}}^R\right|\right](k_z)\,\mathrm{d}k_z. \tag{B.3}$$

It can be easily checked that $\hat{T}_r^R(k_z)$ and $\left[\left|\hat{u}_r^R\right|\right](k_z)$ are real numbers, $\hat{T}_z^R(k_z)$ and $\left[\left|\hat{u}_z^R\right|\right](k_z)$ are imaginary numbers, while $\hat{T}_\theta^R(k_z) = \left[\left|\hat{u}_\theta^R\right|\right](k_z) = 0$. Furthermore, it can be shown that $\hat{\mathbf{T}}^R(-k_z) = \left(\hat{\mathbf{T}}^R(k_z)\right)^*$ and $\left[\left|\hat{\mathbf{u}}^R\right|\right](-k_z) = \left(\left[\left|\hat{\mathbf{u}}^R\right|\right](k_z)\right)^*$. Therefore,

$$E^{\text{img}} = R\int_0^{\infty} \left\{-\left[\left|\hat{u}_r^R\right|\right](k_z)\hat{T}_r^R(k_z) + \left[\left|\hat{u}_z^R\right|\right](k_z)\hat{T}_z^R(k_z)\right\}\mathrm{d}k_z.$$

The final result is given in Equation (18) where we have used the following Wronskian identities in simplification:

$$
\begin{aligned}
J_1\, H_0 - J_0\, H_1 &= \frac{2}{\pi\, k_z} \\
J_1^R\, H_0^R - J_0^R\, H_1^R &= \frac{2}{\pi\, k_z\, R}.
\end{aligned} \tag{B.4}
$$

## APPENDIX C. ASYMPTOTIC BEHAVIOR OF $E^{\text{img}}(r = 1, R)$ at $R \to \infty$

To study the behavior of $E^{\text{img}}(r = 1, R)$ in the limit of $R \to \infty$, it is more convenient to define a new integration variable $x = R\, k_z$, in place of $k_z$. After this variable transformation, the integrand should be written in terms of $x$ and $R$. The integrand can be further simplified in the limit of $R \to \infty$. To do so, we first examine the dependence of various terms in the integrand on $R$ for a fixed $x$. Obviously,

$$
J_0^R \equiv J_0(\mathrm{i}x) \quad J_1^R \equiv J_1(\mathrm{i}x) \quad H_0^R \equiv H_0^{(1)}(\mathrm{i}x) \quad H_1^R \equiv H_1^{(1)}(\mathrm{i}x) \tag{C.1}
$$

are independent of $R$, whereas

$$
\begin{aligned}
J_0 &\equiv J_0(\mathrm{i}x/R) = 1 + \mathcal{O}(R^{-2}) \\
J_1 &\equiv J_1(\mathrm{i}x/R) = \frac{\mathrm{i}\, x}{2\, R} + \mathcal{O}(R^{-3}).
\end{aligned} \tag{C.2}
$$

In the limit of $R \to \infty$, Equation (18) can be reduced to

$$
E_{\text{img}} = \frac{\mu\, b^2\, F(\nu)}{(1-\nu)\, R^3} \tag{C.3}
$$

where

$$
F(\nu) \equiv \int_0^\infty \frac{\tilde{P}(\nu, x)}{\tilde{Q}(\nu, x)}\, \mathrm{d}x \tag{C.4}
$$

$$
\begin{aligned}
\tilde{P}(\nu, x) &= -\frac{\mathrm{i}\pi\, x^4}{2}\left(H_0^{(1)}(\mathrm{i}x) J_0(\mathrm{i}x) + H_1^{(1)}(\mathrm{i}x) J_1(\mathrm{i}x)\right) \\
&+ \frac{x^4}{4} + \frac{3-\nu}{2} x^2 - \mathrm{i}\pi\,(1-\nu) H_1^{(1)}(\mathrm{i}x) J_1(\mathrm{i}x)\, x^2 \\
\tilde{Q}(\nu, x) &= \left(J_0^2(\mathrm{i}x) + J_1^2(\mathrm{i}x)\right) x^2 + 2(1-\nu) J_1^2(\mathrm{i}x).
\end{aligned} \tag{C.5}
$$

The numerical values of $F(\nu)$ for $-1 < \nu < 0.5$ are plotted in Figure 3.

## APPENDIX D. ASYMPTOTIC BEHAVIOR OF $E^{\text{img}}(r = 1, R)$ at $R \to 1$

$E^{\text{img}}$ diverges at $R = 1$ because the integrand of Equation (18) decays too slowly with $k_z$,

$$\frac{P(R=1,k_z)}{Q(R=1,k_z)} = -\frac{1}{k_z} + \mathcal{O}(k_z^{-2}), \quad k_z \to \infty. \tag{D.1}$$

If $R > 1$, then for sufficiently large $k_z$,

$$\frac{P(R,k_z)}{Q(R,k_z)} \to \left[-2(R-1)^2 k_z + 2(R-1) - \frac{1}{k_z}\right] \mathrm{e}^{2(R-1)k_z}, \quad k_z \to \infty, \quad R > 1 \tag{D.2}$$

so that the integral converges. This property of the integrand motivates the following approach to determine the asymptotic behavior of $E^{\text{img}}(r = 1, R)$ for $R \to 1$.

First, we choose a large number $k$ to break the integral of $E^{\text{img}}$ into two parts:

$$E^{\text{img}} = \frac{\mu\, b^2}{2(1-\nu)} \int_0^k \frac{P(R,k_z)}{Q(R,k_z)}\, \mathrm{d}k_z - \frac{\mu\, b^2}{2(1-\nu)} \int_k^\infty \frac{P(R,k_z)}{Q(R,k_z)}\, \mathrm{d}k_z. \tag{D.3}$$

In the limit of $R \to 1$, let $(R-1)^{-1/2} < k < (R-1)^{-1}$, so that $(R-1)k \to 0$ as $R \to 1$. The first integral can be approximated by letting $R = 1$, and the second integral can be approximated by taking the limit of $k_z \to \infty$ for the integrand, i.e.

$$\begin{aligned} E^{\text{img}} &= \frac{\mu\, b^2}{2(1-\nu)} \int_0^k \frac{P(R=1,k_z)}{Q(R=1,k_z)}\, \mathrm{d}k_z \\ &+ \frac{\mu\, b^2}{2(1-\nu)} \int_k^\infty \left[-2(R-1)^2 k_z + 2(R-1) - \frac{1}{k_z}\right] \mathrm{e}^{2(R-1)k_z}\, \mathrm{d}k_z. \end{aligned}$$

The second integral can be evaluated, to terms of $\mathcal{O}((R-1)k)$ analytically:

$$\begin{aligned} &\int_k^\infty \left[-2(R-1)^2 k_z + 2(R-1) - \frac{1}{k_z}\right] \mathrm{e}^{2(R-1)k_z}\, \mathrm{d}k_z \\ &= \left[\frac{1}{2} - (R-1)k\right] \mathrm{e}^{-2(R-1)k} - \mathrm{Ei}(1, 2(R-1)k) \\ &= \ln(2(R-1)k) + \gamma + \frac{1}{2} + \mathcal{O}((R-1)k) \end{aligned} \tag{D.4}$$

where $\gamma = 0.5772156649...$ is the Euler Gamma constant. Therefore, in the limit of $R \to 1$,

$$\frac{E^{\text{img}}}{\mu\, b^2} = \frac{1}{2(1-\nu)} \ln(R-1) + G(\nu) \tag{D.5}$$

$$G(\nu) \equiv \lim_{k\to\infty} \frac{1}{2(1-\nu)} \int_0^k \frac{P(R=1,k_z)}{Q(R=1,k_z)}\,\mathrm{d}k_z + \frac{1}{2(1-\nu)}\left[\ln(2k)+\gamma+\frac{1}{2}\right] \tag{D.6}$$

$$\begin{aligned} P(R=1,k_z) &= 2\pi\,k_z^3(H_0J_0+H_1J_1)J_0J_1 + 2k_z^2(J_1^2-J_0^2) + 4(1-\nu)J_1^2 \\ &+ 4\pi(1-\nu)k_zH_1J_0J_1^2 \end{aligned}$$

$$Q(R=1,k_z) = 2(1-\nu)J_1^2 + (J_0^2+J_1^2)\,k_z^2. \tag{D.7}$$

Due to the divergent integrand, Equation (D.1), the integral in Equation (D.6) diverges as $-\ln k$ in the limit of $k \to \infty$. This divergence is exactly cancelled by the second term (containing $\ln(2k)$) so that Equation (D.6) converges as $k \to \infty$. The numerical values of $G(\nu)$ for $-1 < \nu < 0.5$ are plotted in Figure 3.

## REFERENCES


[1] Hirth, J. P. and Lothe, J. *Theory of Dislocations*, Wiley, New York, 1982.

[2] Bulatov, V. V. and Cai, W. *Computer Simulations of Dislocations*, Oxford University Press, New York, 2006.

[3] Kroupa, F. Circular edge dislocation loop. *Czechoslovak Journal of Physics,* 10B, 284–293 (1960).

[4] Eshelby, J. D. *Boundary problems*, in *Dislocations in Solids*, Vol. 1, pp. 167–221, ed. F. R. N. Nabarro, North-Holland, Amsterdam, 1979.

[5] Freund, L. B. and Suresh, S. *Thin Film Materials: Stress, Defect Formation, and Surface Evolution*, Oxford University Press, New York, 2003.

[6] van der Merwe, J. H. and van der Berg, N. G. Misfit dislocation energy in epitaxial overgrowths of finite thickness. *Surface Science,* 32, 1–15 (1972).

[7] Uchic, M. D., Dimiduk, D. M., Florando, J. N. and Nix, W. D. Sample dimensions influence strength and crystal plasticity. *Science,* 305, 986–989 (2004).

[8] Greer, J. R. and Nix, W. D. Nanoscale gold pillars strengthened through dislocation starvation. *Physical Review B,* 73, 245410 (2006).

[9] Kang, K. and Cai, W. Brittle and ductile fracture of semiconductor nanowires—molecular dynamics simulations. *Philosophical Magazine,* 14–15, 2169–2189 (2007).

[10] Lauhon, L., Gudiksen, M., Wang, D. and Lieber, C. Epitaxial core–shell and core–multishell nanowire heterostructures. *Nature,* 420, 57–61 (2002).

[11] Liang, Y., Nix, W. D., Griffin, P. B. and Plummer, J. D. Critical thickness enhancement of epitaxial SiGe films grown on small structures. *Journal of Applied Physics,* 97, 043519 (2005).

[12] Weinberger, C. R. and Cai, W. Computing image stress in an elastic cylinder. *Journal of the Mechanics and Physics of Solids,* 55, 2027–2054 (2007).

[13] Achenbach, J. D. *Wave Propagation in Elastic Solids*, North-Holland, Amsterdam, 1982.

[14] Barnett, D. M. and Lothe, J. An image force theorem for dislocations in anisotropic bicrystals. *Journal of Physics F: Metal Physics*, 4, 1618–1635 (1974).

[15] Gavazza, S. D. and Barnett, D. M. The image force on a dislocation loop in a bounded elastic medium. *Scripta Metallurgica*, 9, 1263–1265 (1975).